Tight-binding description of the band-edge states in GaAs/AlAs quantum wells and superlattices

J. G. Menchero, T. G. Dargam,* and Belita Koiller
Instituto de Física, Universidade Federal do Rio de Janeiro, Caixa Postal 68.528, 21945-970 Rio de Janeiro, Brazil
(Received 15 June 1999; revised manuscript received 7 February 2000)

We present a tight-binding investigation of the electron and hole band-edge states for GaAs/AlAs heterostructures. Quantum wells are studied near the critical width in which the system undergoes a direct- to indirect-gap transition. Results are compared for first- and second-nearest-neighbor models. For the first hole state both descriptions are in essential agreement. For the first electron state, however, important differences arise. Although the critical width is the same in both models, for the second-nearest-neighbor approach the indirect-gap regime is characterized by the wave function escaping from the well into the AlAs barriers, but keeping the same translational symmetry. In the first-nearest-neighbor case, the transition is characterized by a change in translational symmetry, and the wave function may or may not remain localized in the well. Type II superlattices are considered within the second-nearest-neighbor approach. For increasing thickness of the AlAs region, we show that the lowest electron state symmetry changes from X_z to X_{xy}, as observed experimentally.

I. INTRODUCTION

In the tight-binding (TB) formalism, sometimes important differences arise between models containing only first-nearest-neighbor (1NN) interactions and those which also include second-nearest-neighbor (2NN) interactions. For instance, Freericks and Falicov[1] showed that ''hidden'' symmetries (of a permutational nature) in 1NN models can give rise to ''accidental'' degeneracies (i.e., those that cannot be explained solely on the basis of translational or rotational symmetry). An important example of this kind of degeneracy occurs in zincblende semiconductors, in which the 1NN treatment gives a dispersionless band structure between the X and W points.[2] This makes 1NN parametrizations unsuitable for describing any property or quantity that depends on the effective masses at those points. The 2NN models, in contrast, do not exhibit this anomalous behavior. Another example of a system in which a 2NN treatment is essential is the case of intervalley coupling at superlattice interfaces. Lu and Sham showed that in order to describe such coupling the 2NN hopping terms at the interface must be included.[3] A further advantage of 2NN approaches is that, due to the larger set of parameters, it is in general possible to obtain a better fit to band energies and effective masses.[4]

Curiously, it has been noted that 1NN models may be more suitable for describing certain problems than their 2NN counterparts. For example, Menchero and Boykin[5] conducted a systematic study of acceptor states in $Al_xGa_{1-x}As$ alloys comparing 1NN and 2NN models, and found that the 1NN results were in better agreement with experiment.[6] The explanation was that 1NN approaches are intrinsically more effective at binding the wave function to the impurity potential.

The work by Menchero and Boykin compared 1NN and 2NN models for *point* potentials (impurities). In this work, we extend the investigation to *two-dimensional* potentials by considering the first electron state, $|e_1\rangle$, and the first hole state, $|h_1\rangle$, in GaAs/AlAs quantum wells (QW's). We model the QW by a superlattice with very thick AlAs spacer layers. For the cases in which the wave function is localized in the GaAs, this is an excellent approximation because the wave function is exponentially damped in the AlAs region, effectively decoupling the GaAs wells. When $|e_1\rangle$ escapes to the AlAs layer, however, we may expect some deviations (due to confinement and tunneling) between the superlattice solution considered here and the ideal QW. In particular, the energy and symmetry of the state $|e_1\rangle$ may be sensitive to the AlAs region width.[7]

This work is organized as follows. In Sec. II we describe the real space (TB) approach adopted for the calculation of the band-edge states in heterostructures, contrasting results from 1NN and 2NN models. In Sec. III we investigate the point-group symmetry of the edge states in QW's and superlattices. A summary and general conclusions are given in Sec. IV.

II. TIGHT-BINDING APPROACH FOR EDGE STATES IN HETEROSTRUCTURES

For a bulk zinc-blende semiconductor, the primitive translation vectors are

$$\mathbf{T}_1=\frac{a}{2}(0,1,1),\quad \mathbf{T}_2=\frac{a}{2}(1,0,1),\quad \mathbf{T}_3=\frac{a}{2}(1,1,0), \qquad (1)$$

where a is the lattice parameter. The conventional (fcc) cell contains four lattice points (located at the origin, $\mathbf{T}_1$, $\mathbf{T}_2$, and $\mathbf{T}_3$), with a basis consisting of a group III and a group V element. This cell is then repeated N_x, N_y, and N_z times in the x, y, and z directions, respectively, generating a large supercell containing $8N_xN_yN_z$ atoms in the zinc-blende structure. For the specific heterostructures considered here, we define z as the growth direction and choose $N_z=30$, which corresponds to 60 monolayers (ML). All group V sublattice sites are occupied by As atoms, and in the group III sublattice we assign Ga atoms to the first N ML, and Al

TABLE I. Upper lines give the energy and symmetry of the first electron and hole states calculated for various GaAs well widths W with 2NN and 1NN TB parametrizations. Energies are given in meV, and refer to the origin at the corresponding GaAs bulk band edges: Conduction band edge for $|e_1\rangle$ and valence band edge for $|h_1\rangle$. The symmetry of each state, according to the notation in Fig. 3, is given in parentheses. Lower lines give the bulk electron and heavy hole effective masses at Γ, normalized by the free electron mass, obtained for each parametrization.

	B2NN[a]		V1NN[b]		B1NN[c]	
W(ML)	$\|e_1\rangle$	$\|h_1\rangle$	$\|e_1\rangle$	$\|h_1\rangle$	$\|e_1\rangle$	$\|h_1\rangle$
12	189($\bar{\Gamma}$)	49($\bar{\Gamma}$)	126($\bar{\Gamma}$)	48($\bar{\Gamma}$)	164($\bar{\Gamma}$)	43($\bar{\Gamma}$)
10	235($\bar{\Gamma}$)	65($\bar{\Gamma}$)	160($\bar{\Gamma}$)	64($\bar{\Gamma}$)	165($\bar{X}$)	57($\bar{\Gamma}$)
8	251($\bar{\Gamma}$)	90($\bar{\Gamma}$)	184($\bar{M}$)	87($\bar{\Gamma}$)	165($\bar{X}$)	78($\bar{\Gamma}$)
6	251($\bar{\Gamma}$)	132($\bar{\Gamma}$)	204($\bar{M}$)	126($\bar{\Gamma}$)	165($\bar{X}$)	114($\bar{\Gamma}$)
4	251(Γ)	209($\bar{\Gamma}$)	242($\bar{M}$)	196($\bar{\Gamma}$)	165($\bar{X}$)	181(Γ)
	m_e^*/m_0	m_{hh}/m_0	m_e^*/m_0	m_{hh}/m_0	m_e^*/m_0	m_{hh}/m_0
GaAs	0.07	0.41	0.12	0.41	0.07	0.47
AlAs	0.17	0.50	0.29	0.58	0.14	0.77

[a]Reference 4.
[b]Reference 8.
[c]Reference 9.

atoms to the remaining $M=(60-N)$ ML. Periodic boundary conditions are imposed, thus generating a $(\mathrm{GaAs})_N(\mathrm{AlAs})_M$ superlattice.

For our TB parametrizations, we use those of Vogl *et al.*[8] and of Boykin *et al.*[9] for 1NN, and of Boykin[4] for 2NN, all of which adopt an sp^3s^* basis set. We refer to them as V1NN, B1NN, and B2NN, respectively. Unless otherwise stated, the results presented below for 1NN calculations were obtained within the more traditional and widely employed V1NN parametrization of Ref. 8. We neglect the spin-orbit interaction and add appropriate constants to the diagonal matrix elements to yield the same conduction-band offsets (0.25 eV) for both parametrizations. Within each material of the superlattice, the bulk parameters for GaAs or AlAs are used without modification. At the interface, we take the average for the on-site energies of the As atoms, the (in-plane) As-As hopping, and the (cross-plane) Ga-Al hopping.

Since only the band-edge states are of interest, complete diagonalization of the Hamiltonian is unnecessary. We solve for the band-edge states using an *order-N* algorithm[10] that scales linearly in time with the number of states, making the solution feasible even for extremely large supercells. We determine the desired eigenstate by minimizing the expectation value of $\langle\Psi|(H-E_{ref})^2|\Psi\rangle$, where E_{ref} is a reference energy suitably chosen in the gap region. States $|e_1\rangle$ or $|h_1\rangle$ are obtained for E_{ref} near the conduction or valence edge, respectively. Thus, for each given E_{ref}, the order-N algorithm leads to a *single eigenstate* and eigenvalue. In general, of course, that state may belong to a many-fold degenerate subspace. Our results for the edge states thus obtained through different parametrizations are summarized in Table I.

The spatial distribution of the states along the heterostructure growth direction z is conveniently depicted through a TB analog of the usual envelope function, introduced by Bastard.[12] This function is obtained from the squared TB expansion coefficients, summed for each monolayer over all x and y site coordinates and over all orbitals.[13] In Fig. 1 we plot the TB envelope function squared for state $|e_1\rangle$ within the B2NN parametrization, obtained for a supercell of size $N_x=N_y=2$, and $N_z=30$. For a well width of 10 ML (and above), $|e_1\rangle$ is localized within the GaAs region. This state is nondegenerate and is composed of s, s^*, and p_z orbitals. The valence state $|h_1\rangle$, which is plotted in the inset, is also confined to the well region. State $|h_1\rangle$ is twofold degenerate, and is made up of p_x and p_y orbitals. We calculated the dipole moment of the band-edge transition, and found it to be

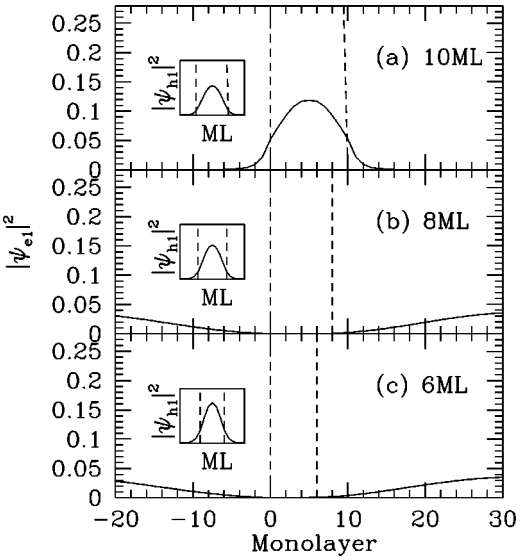

FIG. 1. Tight-binding envelope function squared for the first electron state in a 60 ML GaAs/AlAs superlattice using 2NN parametrization, with the results for the first hole state shown in the inset. For degenerate levels, the distributions were calculated by averaging over all such states. The vertical dashed lines indicate the GaAs/AlAs interfaces. (a) For 10 ML of GaAs, the wave function is localized in the well. For well widths of (b) 8 ML and (c) 6 ML confinement effects expel the electron from the well.

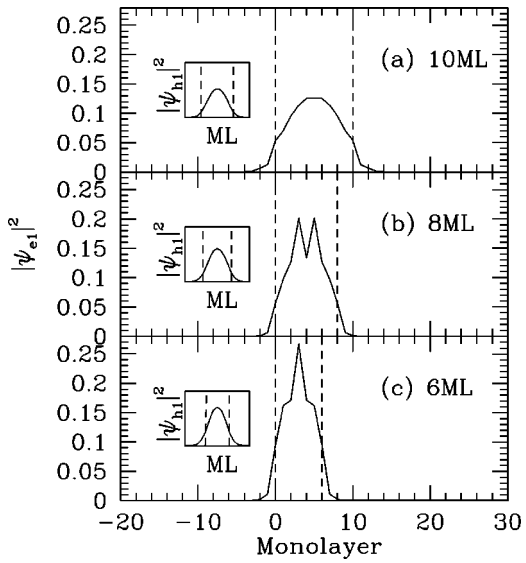

FIG. 2. Tight-binding envelope function squared for the first electron state in a 60 ML GaAs/AlAs superlattice using 1NN parametrization, with the results for the first hole state shown in the inset. For degenerate levels, the distributions were calculated by averaging over all such states. (a) For 10 ML of GaAs, the wave function is localized in the well, in agreement with the 2NN result. For well widths of (b) 8 ML and (c) 6 ML, the transition is indirect, but the wave function remains localized in the well.

strongly optically active. Therefore, QW's of this width are typical type-I materials. For the narrower widths of 8 ML and 6 ML, however, confinement effects expel the electron from the well. The hole state $|h_1\rangle$ remains localized in the well, as shown in the insets, and has essentially the same character as the 10 ML case. The narrower wells, therefore, exhibit typical type-II behavior. These results, including the critical transition width, are in complete agreement with the theoretical results of Franceschetti and Zunger[14] based on an empirical pseudopotential approach.

In Fig. 2 we plot the TB envelope distributions obtained using the V1NN parametrization,[8] for the same size supercell as considered above. The results for both $|e_1\rangle$ and $|h_1\rangle$ states using a well width of 10 ML (and above) are completely consistent with the B2NN case, with both edge states localized inside the well, and a large dipole moment. The behavior of the $|h_1\rangle$ states for 8 ML's and 6 ML's, shown in the insets, are also essentially unchanged from the B2NN case. For the narrower well widths, however, a fundamentally different behavior is observed for $|e_1\rangle$, with the state remaining localized *within* the well. An analysis reveals that for these narrow wells $|e_1\rangle$ is twofold degenerate, and contains contributions from all five sp^3s^* orbitals. Furthermore, the band-edge transition is optically inactive, with *zero* dipole moment. Therefore, the direct-gap to indirect-gap transition occurs at the same critical width for both 1NN and 2NN cases, although the nature of the transition in the wave functions is clearly very different.

It is interesting to note that in the V1NN model[8] the electron remains bound to the QW potential at far narrower widths than in the 2NN case. This result might be interpreted as the two-dimensional analog of that obtained by Menchero and Boykin[5] for point potentials, i.e., 1NN models are more effective at binding than their 2NN counterparts. In order to clarify this question, we have performed calculations with a different 1NN parametrization,[9] which yields improved fits for the electron effective masses. The effective masses for the bulk materials at Γ, obtained for the three parametrizations, are given in Table I. Since V1NN parametrization leads to an electron effective mass almost a factor of two larger than the other models, it is possible that the stronger binding is a consequence of the increased electron effective mass in the GaAs region. Analysis of the $|e_1\rangle$ state obtained with the B1NN parametrization leads to the conclusions that, in the indirect-gap regime, the electron is indeed expelled from the GaAs well, in qualitative agreement with the 2NN results, but the wave function is twofold degenerate, therefore of different translational symmetry than in the 2NN case.

TABLE II. Character table, D_{2d}.

	E	C_{2z}	S_{4z}, S_{4z}^{-1}	C_{2x}, C_{2y}	$\sigma_{110}, \sigma_{1\bar{1}0}$
A_1	1	1	1	1	1
A_2	1	1	1	−1	−1
B_1	1	1	−1	1	−1
B_2	1	1	−1	−1	1
E	2	−2	0	0	0

The relevance of the effective masses may be inferred from the binding energies of the edge states given in Table I. We note that for comparable effective masses, as is the case of B1NN and B2NN for electron states, the binding energies for $W=12$ are in better agreement among each other than the one corresponding to the V1NN parametrization. Similarly, for hole states, the B2NN and V1NN effective masses are in better agreement with each other than with B1NN, leading to corresponding agreements for the binding energies of the $|h_1\rangle$ state. On the other hand, the electron wave function for B1NN is expelled from the GaAs well for widths between 10 and 12 ML, which is wider than in the B2NN parametrization (8–10 ML). This implies that the B1NN is *less* able to bind the electron to the well than B2NN. Therefore, it seems that for QW electron states the 1NN models are *not* intrinsically stronger at binding than the 2NN model, in contrast to the expected behavior based on acceptor levels.[5]

III. POINT-GROUP SYMMETRY OF THE EDGE STATES

A. Quantum wells and type-I superlattices

In order to understand the intriguing results in Sec. II, a more detailed analysis of the wave-function symmetry is required. Information regarding each calculated eigenstate, including degeneracy and symmetry, is obtained within a group-theoretical approach. The point-group symmetry of the superlattice is D_{2d}, which consists of eight operations, and whose character table is given in Table II. Our objective is to obtain all linearly independent eigenfunctions which are degenerate with $|\Psi\rangle$ by reasons of symmetry. We accomplish this by a two-step method. First, we generate the symmetry-related eigenfunctions

$$\mathcal{P}_i|\Psi\rangle = |\Phi_i\rangle, \tag{2}$$

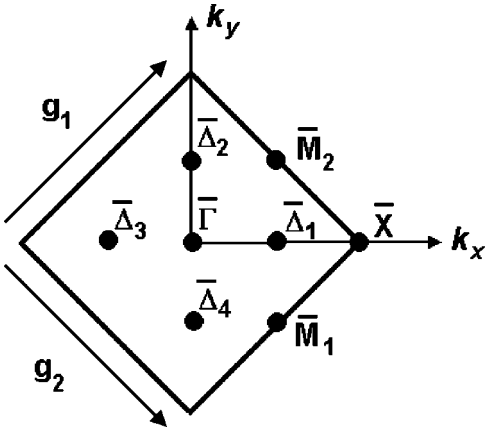

FIG. 3. Two-dimensional Brillouin zone for the quantum well. The sampling for $N_x=N_y=2$ results in the 8 **k** points shown. The reciprocal-lattice vectors for the superlattice are $\mathbf{g}_1$ and $\mathbf{g}_2$.

where the $\mathcal{P}_i$ are the Wigner operators[11] for the point-group elements. These eight eigenfunctions $|\Phi_i\rangle$ are necessarily degenerate, while of course not necessarily linearly independent. The second step, therefore, is to perform a Gram-Schmidt orthonormalization. The dimension of the linearly independent subspace immediately gives the degeneracy of the level.

For the superlattice, the primitive translation vectors are

$$\mathbf{t}_1=\frac{a}{2}(1,1,0),\quad \mathbf{t}_2=\frac{a}{2}(1,-1,0),\quad \mathbf{t}_3=\frac{a}{2}(0,0,N+M), \tag{3}$$

with the reciprocal-lattice vectors given by

$$\mathbf{g}_1=\frac{2\pi}{a}(1,1,0),\quad \mathbf{g}_2=\frac{2\pi}{a}(1,-1,0),\quad \mathbf{g}_3=\frac{2\pi}{a}\left(0,0,\frac{2}{N+M}\right), \tag{4}$$

where we have assumed $N+M$ is even.

As mentioned above, the band-edge states were calculated using a supercell size $N_x=N_y=2$, which corresponds to eight *superlattice* primitive unit cells. We considered larger supercells, ranging up to $N_x=N_y=8$, but found no change in the band-edge eigenenergies. This means that the translational symmetries of the band-edge states correspond to one of the eight **k** points sampled in the superlattice Brillouin zone. The Brillouin zone for an ideal ($N_z\to\infty$) QW is shown in Fig. 3, along with the **k**-point sampling for the $N_x=N_y=2$ supercell.

By examining the expansion coefficients for the wave functions, it is a straightforward matter to deduce their **k** symmetry. For instance, $\bar{\Gamma}$ states are invariant under a translation $\mathbf{t}_1$, whereas $\bar{X}$ states change sign under the same translation. States not obeying either rule must be either $\bar{\Delta}$ or $\bar{M}$. These states can be easily differentiated by considering a translation $2\mathbf{t}_1$, which leads to a sign change for $\bar{\Delta}$ but not $\bar{M}$. From this analysis we find that the $|e_1\rangle$ state for 2NN is $\bar{\Gamma}$ for the three well widths considered in Fig. 1, and also for the $W=10$ ML case for 1NN in Fig. 2. However, for the narrower wells in 1NN, we find that the $|e_1\rangle$ state occurs at $\bar{M}$, for the V1NN parametrization, or at $\bar{X}$, for the B1NN parametrization. In all cases the $|h_1\rangle$ state symmetry is $\bar{\Gamma}$. Translational symmetry therefore explains why the band-edge transition for 1NN is dipole forbidden for $W=8$ ML and $W=6$ ML. It is worth pointing out that none of the degeneracies encountered in this work are of the ''accidental'' type of Freericks and Falicov.[1]

The results presented in Figs. 2(b) and 2(c) are also in contradiction with those obtained by Ihm,[15] who performed TB calculations for GaAs-AlAs superlattices within the same V1NN model adopted here.[8] He finds that, for the GaAs layer thickness below ~ 30 Å, the state $|e_1\rangle$ is confined to the AlAs layer region. Although details of his TB calculations are not presented, we may infer from the above results that his **k**-point sampling included only $\bar{\Gamma}$ and $\bar{X}$ points, as is the case for a $N_x=N_y=1$ supercell.

For the cases in which $|e_1\rangle$ corresponds to $\bar{\Gamma}$, it is also useful to calculate the point-group symmetry, because this determines the dipole selection rules for the lowest-energy transition. The dipole operator can be written as $\vec{r}\cdot\vec{\epsilon}$, where $\vec{r}$ is the position vector and $\vec{\epsilon}$ is the electric field vector. According to the matrix element theorem,[11] $\langle h_1|\vec{r}\cdot\vec{\epsilon}|e_1\rangle$ can be nonzero only if the irreducible representation of $\langle h_1|$ is contained in the direct product of the irreducible representations of $\vec{r}\cdot\vec{\epsilon}$ and $|e_1\rangle$. These symmetries can be easily found by application of the Wigner operators $\mathcal{P}_i$, and comparing the traces for each class of operators to the characters in Table II. We find that for all electron states $|e_1\rangle$ occuring at $\bar{\Gamma}$, in both 1NN and 2NN, the point-group symmetry is A_1. Furthermore, it can be easily verified that for the case $\vec{\epsilon}$ lying in the xy plane, the dipole operator transforms according to E, whereas if $\vec{\epsilon}$ is along z then the irreducible representation is B_2. The relevant direct products can be easily worked out with the aid of the character table

$$E^{\gamma}\otimes A_1^{|e_1\rangle}=E,\quad B_2^{\gamma}\otimes A_1^{|e_1\rangle}=A_1, \tag{5}$$

where γ denotes the irreducible representation of the dipole operator. State $|h_1\rangle$ has point-group symmetry E in all cases considered. Therefore, the matrix element theorem shows that $|e_1\rangle\leftrightarrow|h_1\rangle$ transitions are dipole-allowed only if the field polarization lies in the xy plane.

B. Type-II superlattices

It is interesting to consider more carefully the 2NN case in which the electron state is expelled from the well. Intuitively, it is clear that the $|e_1\rangle$ state must be ''X-like,'' because the conduction band minimum for pure AlAs occurs at X. However, care must be exercised because the three X states that are degenerate in the *bulk*, fold into different points of the *superlattice* Brillouin zone

$$X_z\to\bar{\Gamma},\quad X_x,X_y\to\bar{X}. \tag{6}$$

Therefore, for the case in which the $|e_1\rangle$ state is $\bar{\Gamma}$, the transition is *pseudodirect*, i.e., the transition is dipole allowed but very weak due to the small spatial overlap between the electron and hole wave functions. For $\bar{X}$ the dipole matrix element is identically zero and optical transitions are only possible with phonon assistance.

According to our previous analysis for superlattices of period 60 ML, the $|e_1\rangle$ state is $\overline{\Gamma}$, and so it is clear that this must be derived from the X_z state of the bulk. This can be easily verified by showing that the wave function is invariant under a *bulk* translation vector $\mathbf{T}_3$, but changes sign under $\mathbf{T}_1$ or $\mathbf{T}_2$. For wider wells, i.e., wider AlAs regions in this case, an X_{xy} lowest electron state can be expected because the confinement energy (which favors an X_z symmetry for $|e_1\rangle$) becomes dominated by the effect of intervalley coupling, which pushes an X_{xy} level below X_z. In order to estimate the crossover width, we write the energy of the X_z state in the superlattice as

$$E(X_z)=E_X^0+\frac{\hbar^2\pi^2}{2m_l^*L^2}, \tag{7}$$

where E_X^0 is the energy in the bulk. The second term is the confinement energy assuming infinite and perfectly flat barriers, with $m_l^*=1.34m_e$ being the longitudinal effective mass,[4] and L being the width of the AlAs layer ($L=M$ ML in our supercells). Intervalley coupling between X_x and X_y (which would be otherwise degenerate) will push the two states apart. As a first approximation, the lower-lying state will have an energy

$$E(X_{xy})=E_X^0+\frac{\hbar^2\pi^2}{2m_t^*L^2}-\frac{\Omega_0}{L'}, \tag{8}$$

where $m_t^*=0.26m_e$ is the transverse effective mass,[4] $L'=(N+M)$ ML is the superlattice period, and Ω_0 is the intervalley coupling strength, recently[16] calculated to be 0.39 eV Å. For the narrow GaAs layers considered here, we can safely set $L'\approx L$. Solving for the critical width which pushes an X_{xy} state below X_z, we obtain an AlAs thickness of approximately 100 ML. Experimentally, Kesteren *et al.* found[7] the crossover thickness to be ~ 21 ML. However, in the same studies they showed that *strain effects* lower the E_{xy} level by roughly 23 meV relative to E_z. Including this term into our analysis leads then to a crossover thickness of 22 ML, in excellent agreement with experiment. It is interesting to observe, however, that even in the absence of strain effects, the X_{xy} level is predicted to be the lowest electron state for wide enough spacer layers.

IV. SUMMARY AND CONCLUSIONS

In summary, we have presented a TB study of the edge states for a GaAs QW embedded in AlAs spacer layers, near the critical well width for which the fundamental transition goes from direct (allowed) to indirect (forbidden). We compared 1NN and 2NN models, and found that both provided the same description of the first hole state $|h_1\rangle$ for all widths considered. For the first electron state $|e_1\rangle$, both models were again in agreement for wide enough wells, in the direct-gap regime. For narrower wells, however, important differences arise. Two 1NN parametrizations were considered, and we found that the indirect-gap regime is always characterized by a change in **k** symmetry. For the 2NN model, the indirect-gap regime is characterized by the electron wave function escaping from the GaAs well, but keeping the same **k** symmetry.

Our study also indicates the relevance of proper **k**-point sampling. It was pointed out by Lu and Sham[3] that Ihm's 1NN TB calculation[15] gave an invalid ordering of the X_z level with respect to the X_{xy} due to the infinite transverse effective mass in the X valley of the bulk bands inherent to 1NN TB models. We showed here that, for the 1NN model, not only the relative position of levels in **k** space is affected in the narrow GaAs layer limit, but actually an inversion in the *real space position* of the levels may result when a more complete **k**-point sampling is considered through large enough supercells.

For type II structures, we show that for increasing AlAs barrier width a crossover in the lowest electron state symmetry, from X_z to X_{xy}, is expected. This transition, induced by the X_x-X_y coupling, is predicted to occur even in the absence of strain effects.

ACKNOWLEDGMENTS

We thank R. B. Capaz for interesting discussions and for a critical reading of this manuscript. We also acknowledge helpful assistance from F. J. Ribeiro. This work was supported by CNPq, PRONEX, FAPERJ, and FUJB.

*Present address: Instituto de Física, Universidade Federal Fluminense, 24210-340, Niterói-RJ, Brazil.

[1] J.K. Freericks and L.M. Falicov, Lett. Math. Phys. **22**, 277 (1991); Phys. Rev. B **44**, 2895 (1991).
[2] D.J. Chadi and M.L. Cohen, Phys. Status Solidi B **68**, 405 (1975).
[3] Yan-Ten Lu and L.J. Sham, Phys. Rev. B **40**, 5567 (1989).
[4] T.B. Boykin, Phys. Rev. B **56**, 9613 (1997).
[5] J.G. Menchero and T.B. Boykin, Phys. Rev. B **59**, 8137 (1999).
[6] G. Oelgart, B. Lippold, R. Heilmann, H. Neumann, and B. Jacobs, Phys. Status Solidi A **115**, 257 (1989).
[7] H.W. van Kesteren, E.C. Cosman, P. Dawson, K.J. Moore, and C.T. Foxon, Phys. Rev. B **39**, 13 426 (1989); P. Dawson, C.T. Foxon, and H.W. van Kesteren, Semicond. Sci. Technol. **5**, 54 (1990).
[8] P. Vogl, H.P. Hjalmarson, and J.D. Dow, J. Phys. Chem. Solids **44**, 365 (1983).
[9] T.B. Boykin, G. Klimeck, R.C. Bowen, and R. Lake, Phys. Rev. B **56**, 4102 (1997).
[10] J.K.L. MacDonald, Phys. Rev. **46**, 828 (1934); R.B. Capaz, G.C. de Araújo, B. Koiller, and J.P. von der Weid, J. Appl. Phys. **74**, 5531 (1993); L.W. Wang and A. Zunger, J. Chem. Phys. **100**, 2394 (1994).
[11] M. Tinkham, *Group Theory and Quantum Mechanics* (McGraw-Hill, New York, 1964).
[12] G. Bastard, *Wave Mechanics Applied to Semiconductor Heterostructures* (Les Éditions de Physique, Paris, 1988).
[13] T.G. Dargam and B. Koiller, Solid State Commun. **105**, 211 (1998).
[14] A. Franceschetti and A. Zunger, Phys. Rev. B **52**, 14 664 (1995).
[15] J. Ihm, Appl. Phys. Lett. **50**, 1068 (1987).
[16] J.G. Menchero, B. Koiller, and R.B. Capaz, Phys. Rev. Lett. **83**, 2034 (1999).